Proton Electron Nuclear Double Resonance from Nitrosyl Horse Heart Myoglobin: The Role of His-E7 and Val-E11

Marco Flores, Eliane Wajnberg, and George Bemski
Centro Brasileiro de Pesquisas Físicas, 22290-180 Rio de Janeiro, Brazil

Keywords: Hemoproteins, Rhombic and axial symmetries.

Running title: ^{1}H ENDOR from Nitrosyl Myoglobin.

ABSTRACT

Electron Nuclear Double Resonance (ENDOR) spectroscopy has been used to study protons in nitrosyl horse heart myoglobin (MbNO). ^{1}H ENDOR spectra were recorded for different settings of the magnetic field. Detailed analysis of the ENDOR powder spectra using computer simulation, based on the “orientation-selection” principle lead to the identification of the available protons in the heme pocket. We observe hyperfine interactions of the N(HisF8)-Fe^{2+}-N(NO) complex with five protons in axial and with eight protons in the rhombic symmetry along different orientations including those of the principal axes of the *g*-tensor. Protons from His-E7 and Val-E11 residues are identified in the two symmetries, rhombic and axial, exhibited by MbNO. Our results indicate that both residues are present inside the heme pocket and help to stabilize one particular conformation.

INTRODUCTION

The role of the distal histidine residue, His-E7, in mammalian myoglobins and hemoglobins has been extensively studied since it is thought to be the key residue for regulating oxygen affinity (Olson et al., 1988; Springer et al., 1989; Mathews et al., 1989; Rohlfs et al., 1990). The distal valine, Val-E11, is also of interest because it has contact with both the bound ligand and His-E7, restricting the size of the binding site in these proteins. Several authors have suggested that the Val-E11 residue in both myoglobin and hemoglobin may orient bound oxygen toward the ε-amino nitrogen of His-E7 for more efficient hydrogen bonding and that this close proximity to the bound ligand inhibits CO binding due to the preferred linear Fe-C-O geometry (Perutz 1970, 1989; Phillips 1980; Shaanan 1983).

Three mechanisms have been proposed to account for the ability of myoglobin to stabilize bound O_2 and discriminate against CO binding. First, steric accessibility. The proximity of the distal histidine (His-E7) to the heme iron reduces the CO binding affinity by preventing the formation of the linear Fe-C-O bonding configuration perpendicular to the heme plane that is observed in X-ray crystallographic analysis of model heme CO complexes (Peng and Ibers, 1976). In contrast, the bent configuration favored by O_2 coordination would not be sterically hindered by the distal histidine (Jameson et al., 1978). Second, hydrogen bonding. Neutron diffraction studies of sperm whale myoglobin have revealed a hydrogen bond to bound O_2 but not to bound CO (Phillips and Schoenborn, 1981; Hanson and Schoenborn, 1981). Third, local polarity. Traylor et al. (1985) have shown that solvent composition and local polarity also contribute to the discrimination between CO and O_2.

Since the pioneering experiment of Feher (Feher et al., 1973), who first used the electron-nuclear double resonance (ENDOR) technique in the study of the hemoproteins, many papers have described different aspects of the electronic structure of protons and nitrogens in the region of heme, principally in met- and nitrosyl hemoglobin and myoglobin (Mulks et al., 1979; Scholes et al., 1982; Höhn et al., 1983; Kappl and Hüttermann, 1989; Hüttermann, 1993;

Hüttermann et al., 1994). This was due in great part to the fact that the paramagnetic heme iron-NO system displays a great deal of similarity in its electronic structure to that of the physiologically important heme iron-O_2. The studies in nitrosyl myoglobin (MbNO) and nitrosyl hemoglobin (HbNO) gained in interest when it became evident that these proteins exhibit two different symmetries: axial and rhombic and that their ratio varies with temperature, above 40 K in MbNO (Hüttermann et al., 1994; Flores et al., 1997).

We have examined the role of the pocket histidine and valine in nitrosyl horse heart myoglobin by observing hyperfine interactions between the paramagnetic center and the protons in the distal residues using angle-selected ENDOR spectroscopy. This methodology was first suggested by Rist and Hyde (1970), it permits for proton identifications and has been described (Hoffman et al., 1989, 1993; Hurst et al., 1985) and intensively applied by others authors (Henderson et al., 1985; True et al., 1988; Gurbiel et al., 1993; Moens et al., 1994; Schramm and Rossi, 1999; Tierney et al., 1999; Kappl et al., 1999). The procedures for determining hyperfine tensors using this methodology were developed by Hoffman's group and have been used in this paper (Hoffman et al., 1989, 1993).

In order to interpret the ENDOR spectra, we consider the stereochemical variability of the Fe-NO bond with respect to the porphyrin ring. It follows, that at low temperatures at which ENDOR measurements have to be performed (10 K) one deals always with a superposition of rhombic and axial species and thus, at certain magnetic fields, with a superimposed ENDOR spectra. We are not aware of any work in the literature which studies ENDOR spectra from MbNO in frozen solution and considers the superposition of the rhombic and axial symmetries. In this paper we obtain detailed information about the proton participation in the heme pocket in both symmetries.

EXPERIMENTAL METHODS

Angle-selected ENDOR spectroscopy

Interpretation of powder ENDOR spectra requires initial analysis of the EPR spectrum to determine the relation between molecular orientations and resonant field values. For a more convenient picture, molecular orientation in the applied field defines the field direction in the *g*-axis system. In the heme iron-NO system in nitrosyl heme proteins, one must often consider the *g* and hyperfine anisotropy to determine the field directions that contribute to the EPR spectrum at any given field magnitude. If ENDOR data are collected at a series of EPR field values, the angular dependence of the hyperfine energy can be measured and analyzed to determine the location and contact interaction for ligand nuclei.

The contribution of hyperfine and electron *g* values anisotropy to the EPR spectrum is described by the following equations (Hurst et al., 1985):

$$H_0 = \frac{h\nu - M_I A(\theta,\phi)}{\beta_e g(\theta,\phi)} \tag{1}$$

$$g(\theta,\phi) = [\sum_{i=1}^{3} (g_i h_i)^2]^{1/2} \tag{2}$$

$$A(\theta,\phi) = \frac{[\sum_{i=1}^{3} (\sum_{j=1}^{3} A_{ji} g_j h_j)^2]^{1/2}}{g(\theta,\phi)} \tag{3}$$

$$h_1 = \cos\phi \sin\theta \qquad h_2 = \sin\phi \sin\theta \qquad h_3 = \cos\theta$$

$$\boldsymbol{H} = [h_1, h_2, h_3]\, H_0 \tag{4}$$

where H_0 is the resonant field, h is Planck's constant, ν is the microwave frequency, M_I is the nuclear spin quantum number, and β_e is the Bohr magneton. Angles θ and ϕ are field orientation parameters in the *g*-axes system as shown in Fig. 1. The solution of Eq. 1 gives the θ and ϕ values which contribute to the resonance at any field value. When the *g* and hyperfine anisotropies are axial with coincident axes, the ϕ dependence in Eqs. 1-3 vanishes and resonant field values depend only on the angle θ (Hoffman and Gurbiel, 1989).

ENDOR is performed at fixed field values at which particular sets of molecular orientations are selected. Extraction of nuclear coordinates from the resulting ENDOR spectra is achieved by associating specific field directions with observed ENDOR peaks positions. The equations relating ENDOR frequencies to applied field directions are (Abragam and Bleany, 1970; Thuomas and Lund, 1975; Hutchison and McKay, 1977):

$$\nu(\boldsymbol{H}, m_S) = [\sum_{i=1}^{3} [\frac{m_S}{g(\theta,\phi)} (\sum_{j=1}^{3} g_j h_j A_{ji}) - h_i \nu_0]^2]^{1/2} \tag{5}$$

$$\nu_0 = g_N \beta_N H_0 / h$$

$$A_{ij} = \frac{-\beta_e g_N \beta_N}{h r^3} g_i (3 r_i r_j - \delta_{ij}) + A_{iso} \delta_{ij} \tag{6}$$

where ν ($\boldsymbol{H}$, m_S) is the nuclear resonant frequency, m_S is the electron spin quantum number, ν_0 is the nuclear Larmor frequency. The elements of the hyperfine tensor, A_{ij} are function of the direction cosines (r_i) for the metal-nucleus vector, the metal-nucleus separation r, the principal g values, and the isotropic Fermi contact interaction (A_{iso}). Equations 5 and 6 establish the correspondence between the observed ENDOR frequencies, the applied field vector, and the nuclear position. In the axial case Eq. 6 can be simplified using only the angle between the metal-nucleus vector and the magnetic field vector (Hoffman and Gurbiel, 1989).

The nuclear resonant frequencies of ENDOR spectra depend on the relative orientation of molecules with respect to the applied field. The ENDOR spectra for powders are taken at constant magnetic field where a unique set of field directions in the g-axes system is selected. The nuclear absorption frequencies present at any field value, therefore, are only those that are consistent with the field selected orientations.

If the magnetic field is set to the low-field turning point in the EPR spectrum (g = 2.078) (Flores et al., 1997), one may in principle select a single orientation which would result in a "single-crystal" ENDOR spectrum (Fig. 2, *a*). At fields other than the low-field turning point, one selects orientations at a fixed θ but a range of values of ϕ. In these cases, a two-dimensional

powder average is obtained in the ENDOR simulated spectra as shown in Fig. 2. Interpretation of ENDOR peaks at one magnetic field must be consistent with interpretations at all other field values, placing stringent conditions on peak assignment and nuclear coordinates.

The nuclear hyperfine tensor can have any symmetry or orientation. For the most general case, the tensor is fully asymmetric and it is impossible to find a coordinate system where the hyperfine tensor is diagonal. When the *g* anisotropy is small compared with the average *g* value, the electron and nuclear spins are quantized along the direction of the applied field. Under these conditions, the maximum hyperfine energy occurs for a field pointed along the metal-nucleus vector ($A_{z'z'}$ axis) and the minimum when the field is near the $A_{x'x'}$, $A_{y'y'}$ plane (Hurst et al., 1985) (Fig. 1).

In this paper we will consider a system with small *g* anisotropy in rhombic and axial symmetries and the *A* tensor characteristic of the protons superhyperfine interactions.

Materials and methods

Mb (horse heart; Sigma) was diluted in phosphate buffer (pH 7.0) completely reduced with sodium dithionite and kept in anaerobic conditions with N_2 flux. MbNO was prepared by injection of NO gas.

EPR and ENDOR measurements were performed with a X-band spectrometer (Bruker; ESP 300E) from 4 K to 40 K, using a helium flux cryostat (Oxford; ESR 900) with a temperature controller (Oxford ITC4). The cryostat is provided with a AuFe vs Chromel thermocouple with its measuring junction in the helium flow directly below the sample position.

^{1}H ENDOR spectra were recorded at 10 K for different settings of the magnetic field within the EPR Fe^{2+}-NO spectrum. The EPR spectrum was partially saturated with 10 mW of microwave power, the ^{1}H ENDOR spectra were recorded with a 354 kHz modulation amplitude, 120 W radio frequency power and 50 scans.

GENDOR program was used to simulate the ^{1}H ENDOR spectra (Hoffman et al., 1984, 1985). The program simulates the contribution of each proton independently. The simulated spectra depend on *g*-factors and microwave frequency. The fitting parameters are principal values of *A*, Euler's angles between *g* and *A* tensors, EPR and ENDOR linewidths, and the observed *g*. To simulate the resulting spectra each proton spectrum is multiplied by a factor chosen in a way such that their sum gives the best fit to the experimental data.

The *g*-factors used in the ENDOR simulations were those determined by EPR simulations of MbNO frozen solutions (Flores et al., 1997). The initial proton hyperfine interactions constants and the Euler's angles between *g*-tensor and hyperfine tensor for ENDOR simulations were obtained with the coordinates of α-chain used by Hüttermann et al. (1994).

Since the electron spin density is distributed mainly over three atoms [Fe^{2+}, N(NO), N^{ε}(His-F8)] in a known fashion, we simplify the analysis calculating the position of a reduced spin-center (Wells and Makinen, 1988; Kappl and Hüttermann, 1989). We consider the spin-density distribution of the complex, with 70% of spin density on the Fe^{2+}, 23% on the N(NO) and 7% on the N^{ε}(His-F8) (Doetschman et al., 1980; Utterback et al., 1983)[†] . The hyperfine interactions were calculated with respect to the reduced spin-center using the Eq. 6 for each symmetry. In the axial case we use the simplified approach (Hoffman and Gurbiel, 1989).

After calculating the principal values of *A* for each of the thirteen protons present for both symmetries, we analyze the behavior of the spectrum of each proton at the selected direction. Only five protons in the axial and eight protons in the rhombic symmetry were identified in the spectra. The initial parameters were then iteratively modified in concordance with the powder ENDOR theory to get the best fit to the experimental spectra.

Fig. 6 was generated in the WebLab ViewerPro program. The carboxyl myoglobin (MbCO) atom positions of A_0 conformation (Fig. 6, *c*) and coordinates of MbNO in the axial

[†] In the axial symmetry the reduced spin center is 0.25 Å from iron in the $g_{//}$ direction and in the rhombic symmetry is 0.25 Å from iron in the g_z direction, in both cases above the heme.

symmetry were obtained from Protein Data Bank (PDB) (Yang and Phillips; Brucker et al.), the rhombic symmetry was constructed using the data from MbNO ENDOR and EPR crystals results (Kappl and Hüttermann, 1989; Hori et al., 1981). To model the location of the identified protons, the proton coordinates calculated from ENDOR spectra were introduced in the reference system of the protein for each symmetry and considered as geometric constraints. The THOR program (Pascutti et al., 1999), is then used to optimize the structures (axial and rhombic) and verify which protein conforms is consistent with our proton identifications. For the rhombic symmetry the atoms of the paramagnetic center were also fixed. The final coordinates for each symmetries after the optimization are in very good agreement with the theoretical values from H-C-H dihedral angles and C-H bond lengths (Fig. 6, *a*-*b*).

RESULTS AND DISCUSSION

Fig. 3, *a* shows experimental ^{1}H ENDOR powder spectra of MbNO, at 10 K along the directions corresponding to g = 2.069, 2.0065 and 1.987; these g values were selected because they gave the best resolution. The frequency range between 11.0-18.0 MHz covers proton interactions arising from nuclei in the porphyrin neighborhood. Fig. 3, *b* compares the spectra at 4 K and 40 K, at the intermediate direction corresponding to g = 2.0065. The spectra are temperature independent in the range between 4 K and 40 K, in agreement with Q-band EPR results (Flores et al., 1997).

The magnetic field dependence of ENDOR spectra is reproduced by simulations which involve available protons considering the two different symmetries of the N^{ε}(His-F8)-Fe^{2+}-N(NO) complex (Hüttermann et al., 1994; Flores et al., 1997). We consider only rhombic symmetry at 3245 G and 3256 G and superposition of both symmetries at 3308 G, 3325 G, 3345 G, 3377 G and 3390 G (Fig. 4).

The final simulation parameters are given in Table 1, and gave very good fits to the experimental data (Fig. 4). The simulations indicate that we deal with six non-heme protons in the rhombic symmetry and four non-heme protons in the axial symmetry (Fig. 5 and Fig. 6).

In the rhombic structure the reduced spin-center interacts with HNE2 and HCE1 protons from His-E7 residue, HCG2I and HCG2III protons from Val-E11 residue; HND1 and HCE1 protons from His-F8 and with HCHA and HCHB mesoprotons considered equivalent to HCHC and HCHD respectively. In the axial structure the reduced spin-center interacts with HNE2 proton from His-E7 residue, HCG2II and HCG2III protons from Val-E11 residue, HCE1 proton from His-F8 and with the four mesoprotons considered all equivalent.

Kappl and Hüttermann (1989), studied MbNO in crystals with a single (rhombic) structure and they identified nine protons from His-E7, Val-E11, Phe-CD1 and heme. We did not consider the Phe-CD1 protons because of their large distance from the paramagnetic complex. We focus on the difference between the protons from Val-E11 and identify two protons of His-F8 in the rhombic structure.

In the present work we use as input Hüttermann's proton coordinates for α-chain (Hüttermann et al., 1994). However on the ENDOR scale of experiments of considerably larger accuracy as compared to X-ray cristallography, myoglobin coordinates are not necessarily identical with α-chains of Hb. By iteration we obtain the proton coordinates, the orientation angles (θ_N and ϕ_N, the Euler's angles in the GENDOR program) and the distance r from eq 6 for the rhombic symmetry. In the axial case we only have the θ_N angle from GENDOR program and a distance is easily calculated using the Eq. 6. These coordinates are summarized in the Table 2.

Even with the simplification introduced by the reduced spin-center, we observe differences between both symmetries, with respect to the amino acids interactions in the heme pocket. In the rhombic symmetry the interaction is with two protons from His-E7 while in the axial symmetry only with one. The distance r for the proton HNE2 in the axial symmetry is larger than in the rhombic case even though the intensity of the hyperfine interaction is larger. In

both cases the spin center interacts with two protons from Val-E11, with HCG2I and HCG2III in the rhombic symmetry and with HCG2II and HCG2III in the axial symmetry.

The resulting rhombic conformation is considerably modified when compared to the original one, since the original atomic positions (databank X-ray positions) are for the axial symmetry (Brucker et al.). In the axial case the differences between the observed positions and the X-ray results are less pronounced, and maybe due to use of the solution instead of crystals, or to the low temperature of the ENDOR experiments. The positions of the amino acids obtained here should be checked by other techniques in solution and at low temperature.

From Frauenfelder's experiment (Hong et al., 1990), we know that the ligand in native MbCO can assume three conformations (A_0, A_1, A_3). In the A_0 conformation, the Fe-C-O bond is nearly linear (Lim et al., 1995), a conformation equivalent to the axial conformation in MbNO. Several experiment showed that the His-E7 side chain in native MbCO does not interact with the bound CO in the A_0 substate (Braunstein et al., 1993; Li et al., 1994). Nevertheless our results show that the His-E7 and Val-E11 side chains interact with the NO in the axial conformation (linear bond), and these interactions are more intense than in the rhombic case (Table 1).

This difference can be understood considering that the His-E7 and Val-E11 are inside the heme pocket and help to stabilize the axial conformation in native MbNO, while in the nearly linear A_0 conformation of native MbCO experiments and simulations show that His-E7 side chain is relatively mobile and probably swung out of the distal pocket (Quillin et al., 1992; Jewsbury and Kitagawa, 1994).

On the other hand Braunstein et al. (1993) using Fourier-transform infrared spectroscopy have shown the influence of several His-E7 and Val-E11 mutants of sperm whale MbCO on the CO orientation in MbCO. For most of the mutants, a single *A* substate band is observed, which points to the crucial role of the His-E7 residue in determining the *A* substates spectrum of the bound CO in the native structure. The fact that some of the mutants show more than one stretch band of the bound CO indicates that the appearance of multiple *A* substates is not exclusively

connected to the presence of His-E7. This hypothesis is in agreement with Hüttermann et al. (1994), who using EPR and ENDOR spectroscopies observed both rhombic and axial conformations in nitrosyl tetraphenyl porphyrin-imidazole (NO-TPP-Im) which contains neither His-E7 nor Val-E11 residues, and an imidazole instead of the His-F8.

CONCLUSIONS

The application of ENDOR spectroscopy with its high spectral resolution to the studies of frozen solutions of NO-ligated horse heart myoglobin has brought about a wealth of detailed structural information concerning the protons of the heme-pocket. One ought to remember that frozen solution are closer to the physiological condition than crystals. Conformational equilibrium of rhombic and axial symmetries is observed. According to Frauenfelder the conformational equilibrium is relevant to the protein function (Frauenfelder et al., 1991). Our results complement Kappl's and Hüttermann's paper on MbNO crystals which are in purely rhombic conformation (Kappl and Hüttermann, 1989). It is quite possible that on the ENDOR scale of resolution structural differences between frozen solutions and crystals should appear.

Temperature dependence of Q-band EPR of nitrosyl horse heart myoglobin showed that both rhombic and axial symmetries are present at low temperatures (Flores et al., 1997). Fig. 6 presents the differences between the axial structures of MbCO and MbNO. The proton interactions in MbNO stabilize this orientation. In this work proton ENDOR results show that the His-E7 and Val-E11 residues are present in the heme pocket and help to stabilize the bound NO in the rhombic and axial conformations of MbNO, in contraposition to the usual assumption that only the His-E7 residue is important in the ligand control. Our results show that when both amino acids are present they interact with Fe-NO in either conformation. It is however known that the two conformations can exist also without them (Hüttermann et al., 1994).

These experiments show that the appearance of the rhombic and axial conformations in MbNO can not be explained simply by the presence of His-E7 and Val-E11. Theoretical results

suggest that the ligand orientation is also determined by the proximal histidine (Lim et al., 1995). It has also been suggested by Perutz that another important function of His-E7 is the removal of protons from the distal pocket to prevent autoxidation (Perutz, 1989).

We conclude that even though Frauenfelder's and our experiments can be interpreted in the framework of conformational model for heme proteins, there are questions which still require explanations.

ACKNOWLEDGMENTS

The authors are grateful to Delson Schramn for useful comments; Pedro Pascutti and Alan da Silva for technical assistance and useful comments in the use of the THOR program and CNPq and CAPES for partial support of this work.

REFERENCES

Abragam, A., and B. Bleaney. 1970. Electron Paramagnetic Resonance of Transition Ions. Clarendon Press, Oxford.

Braunstein, D. P., K. Chu, K. D. Egeberg, H. Frauenfelder, J. R. Mourant, G. U. Nienhaus, P. Ormos, S. G. Sligar, B. A. Springer, and R. D. Young. 1993. Ligand binding to heme proteins: III. FTIR studies of His-E7 and Val-E11 mutants of carbonmonoxymyoglobin. *Biophys. J.* 65:2447-2454.

Brucker, E. A., J. S. Olson, M. Ikeda-Saito, and G. N. Phillips Jr. to be published.

Doetschman, D. C., S. A. Schwartz, and S. G. Utterback. 1980. The electron spin distribution in nitrosylhemoglobin. *Chemical Physics.* 49:1-8.

Feher, G., R. A. Isaacson, C. P. Scholes, and R. Nagel. 1973. Electron nuclear double resonance (ENDOR) investigation on myoglobin and hemoglobin. *Ann. N. Y. Acad. Sci.* 222:86-101.

Flores, M., E. Wajnberg, and G. Bemski. 1997. Temperature dependence of Q-band electron paramagnetic resonance spectra of nitrosyl heme proteins. *Biophys. J.* 73:3225-3229.

Frauenfelder, H., S. G. Sligar, and P. G. Wolynes. 1991. The energy landscapes and motions of proteins. *Science.* 254:1598-1603.

Gurbiel, R. J., Y. Fann, K. K. Surerus, M. M. Werst, S. M. Musser, P. E. Doan, S. I. Chan, J. A. Fee, and B. M. Hoffman. 1993. Detection of two hidtidyl ligands to Cu_A of cytochrome oxidase by 35-GHz ENDOR: $^{14,15}N$ and $^{63,65}Cu$ ENDOR studies of the Cu_A site in bovine heart cytochrome aa_3 and cytochromes cca_3 and ba_3 from *Thermus thermophilus*. *J. Am. Chem. Soc.* 115:10888-10894.

Hanson, J. C., and B. P. Schoenborn. 1981. Real space refinement of neutron-diffraction data from sperm whale carbonmonoxy-myoglobin. *J. Mol. Biol*. 153:117-146.

Henderson, T. A., G. C. Hurst, and R. W. Kreilick. 1985. Angle-selected ENDOR spectroscopy. 2. Determination of proton coordinates from a polycrystalline sample of bis (2, 4-pentanedionato) copper(II). *J. Am. Chem. Soc.* 107:7299-7303.

Hoffman, B. M., and R. J. Gurbiel. 1989. Polycrystalline ENDOR patterns from centers with axial EPR spectra. General formulas and simple analytic expressions for deriving geometric information from dipolar coupling. *J. Magn. Reson.* 82:309-317.

Hoffman, B. M., J. Martinsen, and R. A. Venters. 1984. General theory of polycrystalline ENDOR patterns. ***g*** and hyperfine tensors of arbitrary symmetry and relative orientation. *J. Magn. Reson.* 59:110-123.

Hoffman, B. M., R. A. Venters, and J. Martinsen. 1985. General theory of polycrystalline ENDOR patterns. Effects of finite EPR and ENDOR component linewidths. *J. Magn. Reson*., 62, 537-542.

Hoffman, B. M., R. J. Gurbiel, M. M. Werst, and M. Sivaraja. 1989. Electron nuclear double resonance (ENDOR) of metalloenzymes. Advanced EPR, Applications in biology and biochemistry. A. J. Hoff, editor. Elsevier. 541-591.

Hoffman, B. M., V. J. DeRose, P. E. Doan, R. J. Gurbiel, A. L. P. Houseman, and J. Telser. 1993. Metalloenzyme active-site structure and function through multifrequency CW and pulsed ENDOR. Biological Magnetic Resonance, vol. 13. L. J. Berliner and J. Reuben, editors. Plenum Press, New York and London. 151-218.

Höhn, M., J. Hüttermann, J. C. W. Chien, and L. C. Dickinson. 1983. ^{14}N and ^{1}H ENDOR of Nitrosylhemoglobin. *J. Am. Chem. Soc.* 105:109-115.

Hong, M. K., D. Braunstein, B. R. Cowen, H. Frauenfelder, I. E. T. Iben, J. R. Mourant, P. Ormos, R. Scholl, A. Schulte, P. J. Steinbach, A. H. Xie, and R. D. Young. 1990. Conformational substates and motions in myoglobin. *Biophys. J.* 58:429-436.

Hori, H., M. Ikeda-Saito, and I. Yonetani. 1981. Single crystal EPR of myoglobin nitroxide. *J. Biol. Chem.* 256:7849-7855.

Hurst, G. C., T. A. Henderson, and R. W. Kreilick. 1985. Angle-selected ENDOR spectroscopy. 1. Theoretical interpretation of ENDOR shifts from randomly orientated transition-metal complexes. *J. Am. Chem. Soc.* 107:7294-7299.

Hutchison, C., and D. B. McKay. 1977. The determination of hydrogen coordinates in lanthanum nicotinate dihydrate crystals by Nd^{+3}-proton double resonance. *J. Chem. Phys.* 66:3311-3330.

Hüttermann, J. 1993. ENDOR of randomly oriented mononuclear metalloproteins, Toward structural determinations of the prosthetic group. Biological Magnetic Resonance, vol. 13. L. J. Berliner and J. Reuben, editors. Plenum Press, New York and London. 219-252.

Hüttermann, J., C. Burgard, and R. Kappl. 1994. Proton ENDOR from randomly oriented NO-ligated haemoglobin: Approaching the structural basis for the R-T transition. *J. Chem. Soc. Faraday Trans.* 90:3077-3087.

Jameson, G. B., F. S. Molinaro, J. A. Ibers, J. P. Collman, J. I. Branman, E. Rose, and K. S. Suslick. 1978. Structural-changes upon oxygenation of an iron (II) (porphyrinato) (imidazole) complex. *J. Am. Chem. Soc.* 100:6769-6770.

Jewsbury, P., and T. Kitagawa. 1994. The distal residue-CO interaction in carbonmonoxy myoglobins: A molecular dynamics study of two distal histidine tautomers. *Biophys. J.* 67:2236-2250.

Kappl, R., and J. Hüttermann. 1989. An ENDOR study of nitrosyl myoglobin single crystals. *Isr. J. Chem.* 29:73-84. Kappl, R., and J. Hüttermann. 1989. Heme-globin interactions in nitrosyl-ligated hemoglobin as probed by ENDOR spectroscopy. Advanced EPR, Applications in biology and biochemistry. A. J. Hoff, editor. Elsevier. 501-540.

Kappl, R., S. Ciurli, C. Luchinat, and J. Hüttermann. 1999. Probing structural and electronic properties of the oxidized $[Fe_4S_4]^{3+}$ cluster of *Ectothiorhodospira halophila* iso-II high-potential iron-sulfur protein by ENDOR spectroscopy. *J. Am. Chem. Soc.* 121:1925-1935.

Li, T., M. L. Quillin, G. N. Phillips Jr., and J. S. Olson. 1994. Structural determinants of the stretching frequency of CO bound to myoglobin. *Biochemistry.* 33:1433-1446.

Lim, M., T. A. Jackson, and P. A. Anfinrud. 1995. Binding of CO to myoglobin from a heme pocket docking site to form nearly linear Fe-C-O. *Science*. 269:962-966.

Mathews, A. J., R. J. Rohlfs, J. S. Olson, J. Tame, J. P. Renaud, and K. Nagai. 1989. The effects of E7 and E11 mutations on the kinetics of ligand-binding to R-state human-hemoglobin. *J. Biol. Chem.* 264:16573-16583.

Moens, P. D., F. J. Callens, and P. F. Matthys. 1994. ^{31}P and ^{1}H powder ENDOR and molecular orbital study of a CO_3^{3-} ion in X-irradiated carbonate containing hydroxyapatites. *J. Chem. Soc. Faraday Trans.* 90:2653-2662.

Mulks, C. F., C. P. Scholes, L. C. Dickinson, and A. Lapidot. 1979. Electron nuclear double resonance from high- and low-spin ferric hemoglobins and myoglobins. *J. Am. Chem. Soc.* 101:1645-1654.

Olson, J. S., A. J. Mathews, R. J. Rohlfs, B. A. Springer, K. D. Egeberg, S. G. Sligar, J. Tame, J. P. Renaud, and K. Nagai. 1988. The role of the distal histidine in myoglobin and hemoglobin. *Nature*. 336:265-266.

Pascutti, P. G., K. C. Mundim, A. S. Ito, and P. M. Bisch. 1999. Polarization effects on peptide conformations at molecular dynamics simulation. *J. Comp. Chem.* 20:971-982.

Peng, S. M., and J. A. Ibers. 1976. Stereochemeistry of carbonyl metalloporphyrins-structure of (pyridine) (carbonyl) (5, 10, 15, 20-tetraphenylporphinato) iron (II). *J. Am. Chem. Soc.* 98:8032-8036.

Perutz, M. F. 1970. Stereochemistry of cooperative effects in haemoglobin. *Nature.* 228:726-734.

Perutz, M. F. 1989. Myoglobin and hemoglobin-role of distal residues in reactions with heme ligands. *Trends Biochem. Sci.* 14:42-44.

Phillips, S. E. V. 1980. Structure and refinement of oxymyoglobin at 1.6 Å resolution. *J. Mol. Biol.* 142:531-554.

Phillips, S. E. V., and B. P. Schoenborn. 1981. Neutron-diffraction reveals oxygen-histidine hydrogen-bond in oxymyoglobin. *Nature.* 292:81-82.

Quillin, M. L., R. E. Brantley Jr., K. A. Johnson, and G. Phillips. 1992. Kinetic and structural analysis of the effects of pH on carbon monoxide association in myoglobin. *Biophys. J.* 61:A466.

Rist, G. H., and J. S. Hyde. 1970. Ligand ENDOR of metal complexes in powders. *J. Chem. Phys.* 52:4633-4643.

Rohlfs, R. J., A. J. Mathews, T. E. Carver, J. S. Olson, B. A. Springer, K. D. Egeberg, and S. G. Sligar. 1990. The effects of amino-acid substitution at position-E7 (residue-64) on the kinetics of ligand-binding to sperm whale myoglobin. *J. Biol. Chem.* 265:3168-3176.

Scholes, C. P., A. Lapidot, R. Mascarenhas, T. Inubushi, R. A. Isaacson, and G. Feher. 1982. Electron nuclear double resonance (ENDOR) from heme and histidine nitrogens in single crystals of aquometmyoglobin. *J. Am. Chem. Soc.* 104:2724-2735.

Schramm, D. U., and A. M. Rossi. 1999. EPR and ENDOR studies on CO^- radicals in γ-irradiated synthetic hydroxyapatites. *Phys. Chem. Chem. Phys*. 1:2007-2012.

Shaanan, B. 1983. Structure of human oxyhemoglobin at 2.1 Å resolution. *J. Mol. Biol*. 171:31-59.

Springer, B. A., K. D. Egeberg, S. G. Sligar, R. J. Rohlfs, A. J. Mathews, and J. S Olson. 1989. Discrimination between oxygen and carbon-monoxide and inhibition of autooxidation by myoglobin-site-directed mutagenesis of the distal histidine. *J. Biol. Chem.* 264:3057-3060.

Thuomas, K., and A. Lund. 1975. Evaluation of hyperfine and quadrupole tensors from ENDOR measurements on single crystals. *J. Magn. Reson.* 18:12-21.

Tierney, D. L., H. Huang, P. Martasek, B. S. S. Masters, R. B. Silverman, and B. M. Hoffman. 1999. ENDOR spectroscopic evidence for the position and structure of N^G-hydroxyl-L-arginine bound to holo-neuronal nitric oxide synthase. *Biochemistry*. 38:3704-3710.

Traylor, T. G., N. Koga, and L. A. Deardruff. 1985. Structural differentiation of CO and O_2 binding to iron porphyrins-polar pocket effects. *J. Am. Chem. Soc.* 107:6504-6510.

True, A. E., M. J. Nelson, R. A. Venters, W. H. Orme-Johnson, and B. M. Hoffman. 1988. ^{57}Fe hyperfine coupling tensors of the FeMo cluster in *Azotobacter vinelandii* MoFe protein: Determination by polycrystalline ENDOR spectroscopy. *J. Am. Chem. Soc.* 110:1935-1943.

Utterback, S. G., D. C. Doetschman, J. Szumowski, and A. K. Rizos. 1983. EPR study of the structure and spin distribution at the binding site in human nitrosylhemoglobin single crystals. *J. Chem. Phys.* 78:5874-5880.

Wells, G. B., and M. W. Makinen. 1988. ENDOR determined molecular geometries of spin-labeled fluoranilides in frozen solution. *J. Am. Chem. Soc.* 110:6343-6352.

Yang, F., and G. N. Phillips Jr. to be published.

TABLE CAPTIONS

TABLE 1 Fitting parameters of proton ENDOR simulations and their assignment to specific protons in nitrosyl horse heart myoglobin.

TABLE 2 Coordinates of the protons in the *g*-axis system, obtained from the simulation parameters. These coordinates are with respect to the reduced spin-center.

FIGURE CAPTIONS

FIGURE 1 Coordinate system for EPR and ENDOR calculations showing the applied magnetic field vector and nuclear position (N) in the *g*-axis system. The *A*-axis system is also shown. In our case *r* connects the proton position and the reduced spin-center. It is defined in the heme system with g_x connecting the pyrrols NI, NIII, and g_y conecting NII, NIV; g_z is the heme normal for the axial symmetry. In the rhombic case g_z is titled from the plane normal by 35^0, g_x connects the pyrrols NI and NIII, and g_y is normal to plane $g_x g_z$.

FIGURE 2 Simulated ENDOR spectra. (*a*) Orientation dependence of spectra for the proton HNE2 (His-E7) for rhombic symmetry, directions correspond to the *g* values indicated. (*b*) Spectra of three different protons around the paramagnetic complex at a magnetic field corresponding to an intermediate direction ($g = 2.0065$) for the axial symmetry and (*c*) rhombic symmetry.

FIGURE 3 (*a*) Experimental proton ENDOR spectra at 10 K, at magnetic fields corresponding to the *g* values indicated. (*b*) Proton ENDOR spectra at $g = 2.0065$, at 4 K and 40 K.

FIGURE 4 Experimental and simulated proton ENDOR spectra at 10 K at different magnetic field values (see Table 1 for fitting parameeters). The free proton line is also seen.

FIGURE 5 Typical composition of simulated ENDOR spectra, at 3345 G. The five upper components correspond to the axial structure and the eight lower components correspond to the rhombic structure.

FIGURE 6 Positions of protons identified (●) from the ENDOR spectra. The coordinates were calculated from ENDOR simulations for (*a*) axial and (*b*) rhombic symmetries. (*c*) Carboxyl myoglobin (MbCO) in the A_0 conformation.[43] Figures generated with WebLab ViewerPro program (see material and methods). ● Iron, ● Carbon, ● Nitrogen, ● Oxygen and ● Hydrogen. (1) His-E7, (2) His-F8 and (3) Val-E11.

Rhombic symmetry			
g-factors	g_{xx} = 2.078	g_{zz} = 2.005	g_{yy} = 1.982
Hyperfine coupling	$\boldsymbol{A_{xx}}$ (MHz)	$\boldsymbol{A_{zz}}$ (MHz)	$\boldsymbol{A_{yy}}$ (MHz)
HNE2 (His-E7)	-4.2	2.57	1.3
HCE1 (His-E7)	-0.36	-0.38	0.68
HCG2I (Val-E11)	1.47	-0.73	1.47
HCG2III (Val-E11)	0.7	0.7	-0.35
HND1 (His-F8)	-2.07	-0.25	-0.9
HCE1 (His-F8)	-2	1.13	-4.4
HCHA, HCHC (heme)	-0.95	-0.6	1.9
HCHB, HCHD (heme)	1.5	-0.71	-0.71
Axial symmetry			
g-factors	$g_{//}$ = 2.030	$g_{\perp}$ = 1.976	
Hyperfine coupling	$\boldsymbol{A_{//}}$ (MHz)	$\boldsymbol{A_{\perp}}$ (MHz)	
HNE2 (His-E7)	5.8	-2.9	
HCG2II (Val-E11)	3.7	-1.6	
HCG2III (Val-E11)	2.1	-1.2	
HCE1 (His-F8)	3.35	-4.8	
mesoprotons	1.1	-0.55	

Table 1

Rhombic symmetry			
Protons	θ_N (°)	ϕ_N (°)	r (Å)
HNE2 (His-E7)	52	71	2.72
HCE1 (His-E7)	61	57	4.17
HCG2I (Val-E11)	62	46	3.88
HCG2III (Val-E11)	55	31	4.19
HND1 (His-F8)	142	54	4.44
HCE1 (His-F8)	155	64	3.48
HCHA, HCHC	75	81	4.32
HCHB, HCHD	86	1	4.80
Axial symmetry			
Protons	θ_N		r (Å)
HNE2 (His-E7)	30		3.35
HCG2II (Val-E11)	42		3.99
HCG2III (Val-E11)	24		4.68
HCE1 (His-F8)	116		3.46
heme	90		5.89

Table 2

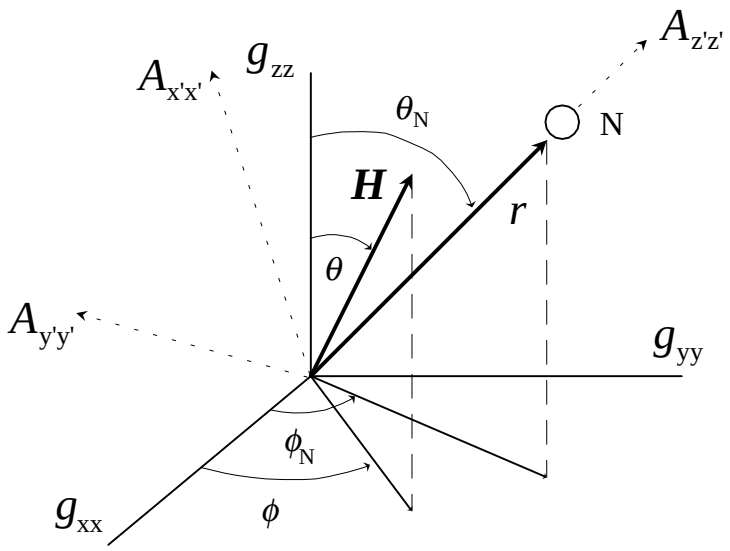

Fig. 1

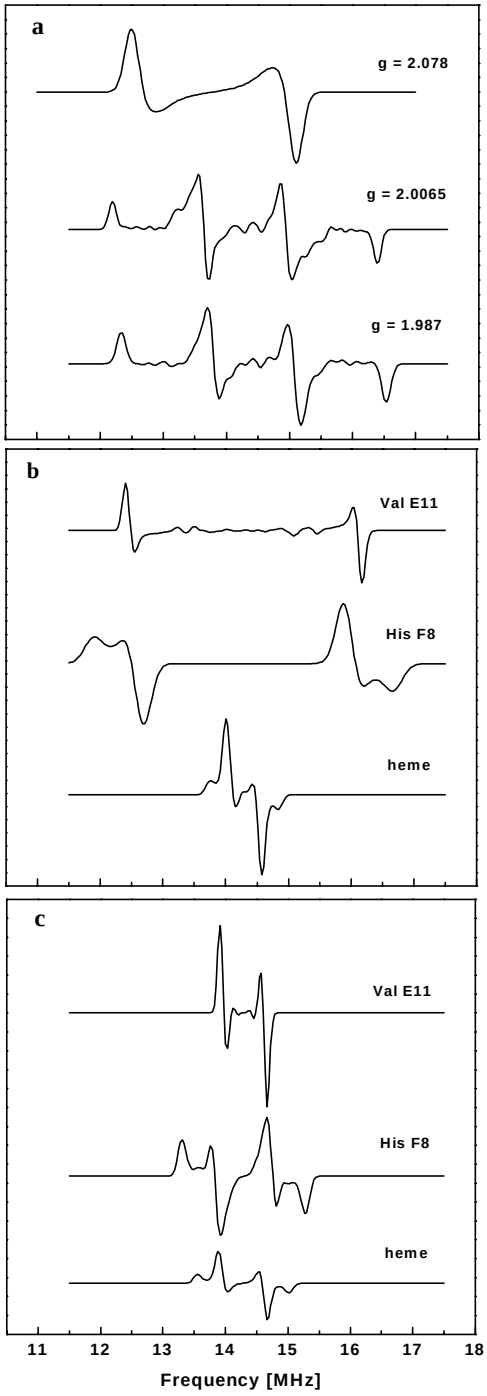
a
g = 2.078
g = 2.0065
g = 1.987
b
Val E11
His F8
heme
c
Val E11
His F8
heme
11
12
13
14
15
16
17
18
Frequency [MHz]

Fig. 2

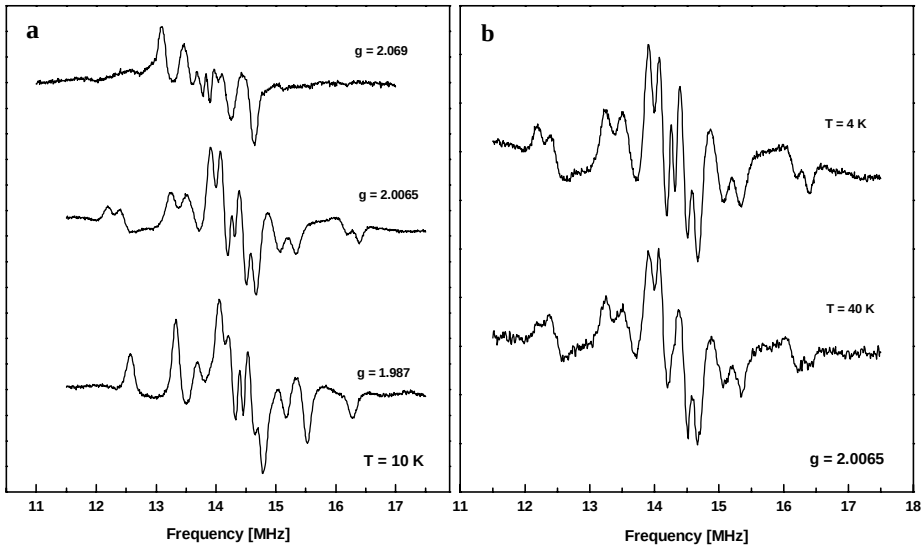
a
g = 2.069
g = 2.0065
g = 1.987
T = 10 K
11 12 13 14 15 16 17
Frequency [MHz]
b
T = 4 K
T = 40 K
g = 2.0065
11 12 13 14 15 16 17 18
Frequency [MHz]

Fig. 3

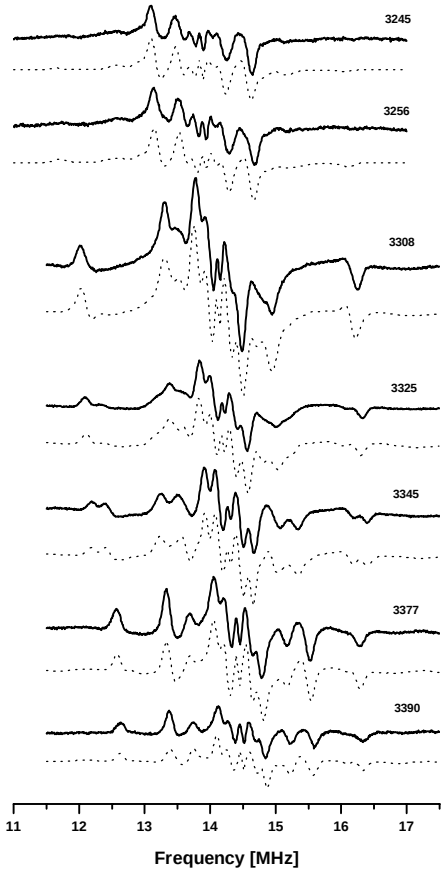
3245
3256
3308
3325
3345
3377
3390
11
12
13
14
15
16
17
Frequency [MHz]

Fig. 4

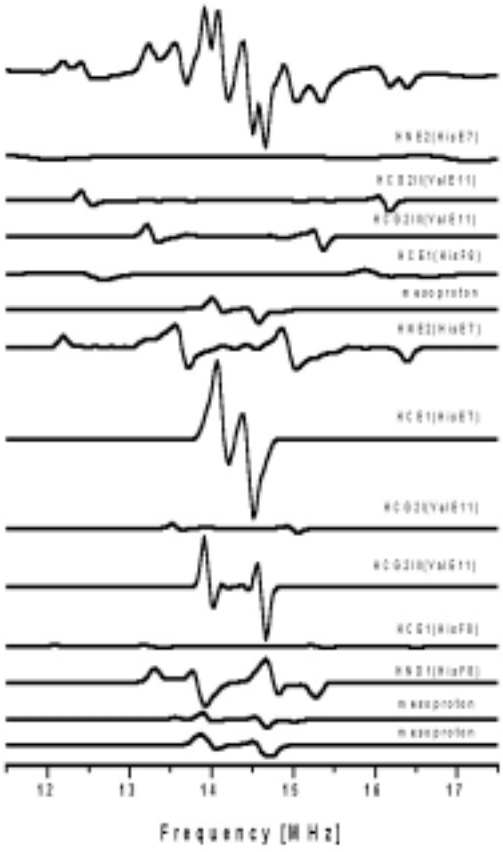
HN E2(HisE7)
HC D2(ValE11)
HC D2(ValE11)
HC E1(HisF8)
HN E2(HisE7)
HC E1(HisE7)
HC D2(ValE11)
HC D2(ValE11)
HC D1(HisF8)
HN D1(HisF8)
12
13
14
15
16
17
Frequency [MHz]

Fig. 5

(a)

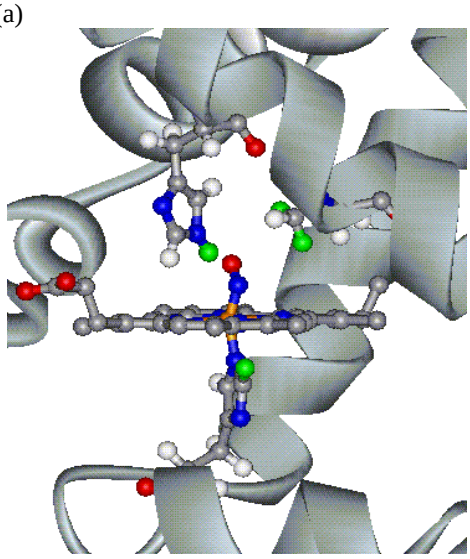

(b)

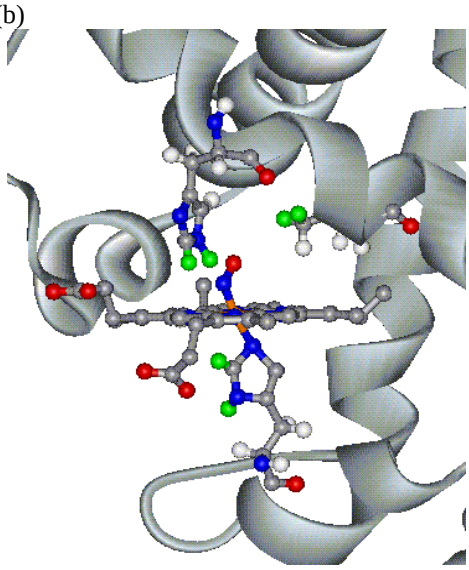

(c)

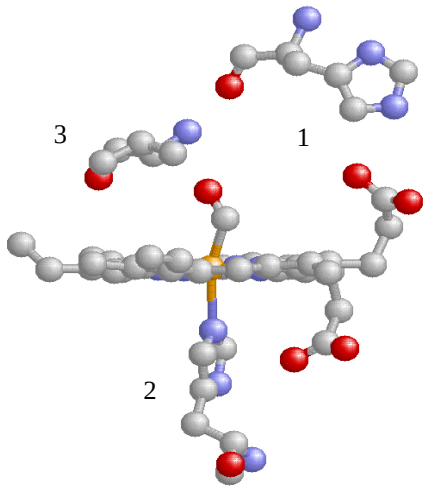

Fig. 6